communications biology

Article

https://doi.org/10.1038/s42003-024-06792-4

Small GTP-binding protein GDP dissociation stimulator influences cisplatin-induced acute kidney injury via PERK-dependent ER stress

Yuxue Yang[1,2,8], Ting Xiong[3,8], Ti Wang[1,8], Xiwei Chen[1], Ziwei Ma[4], Bangyun Zuo[1], Dong Ning[5], Ruilong Song[6], Xuesong Liu[7] ✉ & Daxin Wang[1] ✉

Cisplatin is a common anticancer drug, but its frequent nephrotoxicity limits its clinical use. Small GTP-binding protein GDP dissociation stimulator (smgGDS), a small GTPase chaperone protein, was considerably downregulated during cisplatin-induced acute kidney injury (CDDP-AKI), especially in renal tubular epithelial cells. SmgGDS-knockdown mice was established and found that smgGDS knockdown promoted CDDP-AKI, as demonstrated by an increase in serum creatine, blood urea nitrogen levels and the appearance of tubular patterns. RNA sequencing suggested that protein kinase RNA-like ER kinase (PERK), which bridges mitochondria-associated ER membranes, was involved in smgGDS knockdown following CDDP-AKI, and then identified that smgGDS knockdown increased phosphorylated-PERK in vivo and in vitro. Furthermore, we confirmed that smgGDS deficiency aggravated apoptosis and ER stress in vivo and in vitro. And the ER stress inhibitor 4-Phenylbutyric acid and the inhibition of PERK phosphorylation mitigated smgGDS deficiency-induced ER stress related apoptosis following cisplatin treatment, while the eIF2α phosphorylation inhibitor could not reverse the smgGDS deficiency accelerated cell death. Furthermore, the over-expression of smgGDS could reverse the ER stress and apoptosis caused by CDDP. Overall, smgGDS regulated PERK-dependent ER stress and apoptosis, thereby influencing renal damage. This study identified a target for diagnosing and treating cisplatin-induced acute kidney injury.

Acute kidney injury (AKI), a fatal disease with high mortality and morbidity, is characterized by sudden renal dysfunction[1]. It is responsible for 10–15% of hospitalizations, with 20% requiring kidney replacement therapy[2,3]. The etiology of AKI is complex and includes trauma, sepsis, circulation load changes, and nephrotoxic substances[4]. Cisplatin (cis-diamminedichloroplatinum II, CDDP) is a common anticancer drug, but its side effects include damage to the proximal tubules of the kidneys, neurons, and ears and nephrotoxicity resulting from renal biotransformation disorder due to CDDP accumulation in the kidney. These side effects limit the use of CDDP for treating malignant tumors[5,6]. Research on CDDP-induced AKI (CDDP-AKI) may help identify the mechanism underlying the nephrotoxic effect of the CDDP, provide biomarkers, and alleviate the renal injury induced by CDDP-AKI[7].

Under stressful conditions, an imbalance in cellular homeostasis results in unfolded, misfolded, or dysfunctional proteins accumulating in the endoplasmic reticulum (ER) lumen and an uptick in the unfolded protein response (UPR), causing ER stress[8]. CDDP increases cellular stress, including ER stress, mitochondrial stress, and autophagy, and when this

[1]The Hospital Affiliated to the Medical School of Yangzhou University (Taizhou People's Hospital), No. 366 Taihu Road, Taizhou, Jiangsu, 225300, China. [2]Children's Nutrition Research Center, Department of Pediatrics, Baylor College of Medicine, One Baylor Plaza, Houston, TX, USA. [3]Division of Cardiology, Nanjing First Hospital, Nanjing Medical University, 68 Changle Road, Nanjing, 210006, China. [4]Clinical Medical College, Dalian Medical University, Dalian, Liaoning, 116044, China. [5]School of Medicine, National University of Ireland Galway, University Road, Galway, 999014, Ireland. [6]College of Veterinary Medicine, Yangzhou University, #88 South University Avenue, Yangzhou, Jiangsu, 225009, China. [7]Department of Cardiology, The First Affiliated Hospital of Kunming Medical University, Kunming, 650032, China. [8]These authors contributed equally: Yuxue Yang, Ting Xiong, Ti Wang. ✉e-mail: seanxsl712@163.com; daxinw113@gmail.com

stress exceeds certain thresholds, nuclear fragmentation and cell death occur[9,10]. The ER transmembrane sensors, including protein kinase RNA-like ER kinase (PERK), hepatic activating transcription factor (ATF) 6, and inositol-requiring enzyme 1, are principally responsible for activating ER stress. Furthermore, the intraluminal structures of sensors are tied with are bound and rendered inactive by glucose-regulated protein 78 (GRP78, also known as BiP) under physiological conditions. However, GRP78 is recruited to improperly modified proteins while being separated from the UPR sensor, causing ER stress activation[11]. Moreover, PERK signaling is initiated in response to ER stress via a mechanism involving PERK dimerization and PERK structural domain autophosphorylation[12]. PERK is primarily localized in the ER membrane and acts as a bridge in mitochondria-associated ER membranes (MAMs)[12]. Overactivation of the PERK pathway causes defects in ER stress-induced apoptosis[13,14]. PERK dimerization and structural domain autophosphorylation activate the classical PERK/eukaryotic initiation factor 2α (eIF2α)/C/EBP homologous protein (CHOP) pathway[15]. On the one hand, CHOP could act as a transcription factor to upregulate the expression of BH3-only proteins (e.g., Bim), leading to BAX activation, which mediates mitochondrial apoptosis[13]. On the other hand, CHOP binds to ER and mitochondria and enables the rapid transfer of damage signals from the ER to the mitochondria, thereby exacerbating mitochondria-dependent apoptosis[16]. When eIF2α is activated, it phosphorylates and decreases overall translation and enhances the translation of a subset of genes, such as CHOP and ATF4[16]. The homeostasis of ER influences cell destiny and is highly essential in CDDP-AKI.

Statins can mitigate CDDP-induced renal injury[17,18], and small GTP-binding protein GDP dissociation stimulator (smgGDS, also known as Rap1GDS) has been identified as a crucial mediator of the pleiotropic effects of statins independent of their cholesterol-lowering effects[19–22]. SmgGDS was discovered in 1990; it can regulate the conversion of GDP-bound inactive small GTPases to GTP-bound active small GTPase[23]. The role and function of smgGDS in various diseases have received increasing attention. Statin administration increases smgGDS protein levels and exerts a protective effect against angiotensin-induced hypertrophic cardiomyopathy and endothelial cell injury by reducing oxidative stress levels via RAC1 degradation[19,20]. Additionally, *smgGDS* knockdown results in aortic inflammation and elevated matrix metalloproteinases, which accelerates thoracic aortic aneurysm; however, the local administration of the *smgGDS* gene construct inhibits thoracic aortic aneurysm growth[24]. Moreover, the smgGDS was been identified as the key mediator of sex differences in resilience to ferroptosis in takotsubo syndrome induced heart injury[25]. Lastly, clinical studies have demonstrated that smgGDS mutations are a potential cause of diabetes and hypotonia[26]. SmgGDS plays a primary role in the prenylation of related small GTPases and their translocation to the ER or cell membrane. Moreover, splice switching—an oncogenic ratio of smgGDS isoforms—modifies PERK activity, upregulates ER stress-related CHOP expression, and ultimately enhances Caspase-3 activation and apoptosis[26]. These findings suggest that smgGDS might play a role in human disease and CDDP-AKI. However, studies on smgGDS in kidney-related illnesses are limited.

The precise mechanisms by which smgGDS regulates PERK is required to be clarified. Existing research on the role of smgGDS has mostly focused on cancer-related diseases; however, in recent years, attention has gradually shifted to the role of smgGDS in other areas of human disease, as it may be a potential therapeutic target for kidney disease, cardiovascular disease, and metabolic imbalances. In this study, we hypothesized that smgGDS would regulate PERK expression and/or activity, thereby influencing ER stress and apoptosis in CDDP-AKI.

Results

SmgGDS might play a vital role in CDDP-AKI and tubular epithelial cell death

First, smgGDS expression was confirmed in the kidney using western blotting, and the heart, aorta, and related cell lines were used as a positive control (Fig. S1a). Furthermore, the cisplatin induced AKI model was established by C57BL/6 J mice and the blood and kidney samples were collected. Subsequently, kidney sections were subjected to Hematoxylin and Eosin (HE) as well as periodic acid-Schiff (PAS) staining, followed by kidney injury scoring, and measurement of serum creatinine (SCr) and blood urea nitrogen (BUN). The results showed that after injected with cisplatin (20 mg/kg) 72 h, renal tubule damage ensued, presenting a tubular pattern, with an elevated injury score, BUN, and SCr levels compared to the saline-treated group. These results suggested successful establishment of the CDDP-AKI model (Fig. 1a–d). Furthermore, immunofluorescence and western blotting were conducted to identify smgGDS alterations in CDDP-AKI. Immunofluorescence analysis showed that smgGDS expressed in kidney, specifically that expressed in the renal tubular epithelial cells (the cadherin-16-positive cells), was reduced in the CDDP-AKI group compared with that in the saline-treated group in vivo (Fig. 1e). Additionally, smgGDS was mainly expressed in renal tubular epithelial cells (Fig. 1e). Renal tubular epithelial cell lesions—an important pathophysiological process in AKI and TCMK-1—were selected for further study. Next, immunofluorescence analysis demonstrated that smgGDS decreased in CDDP-treated TCMK-1 cells compared with that in control cells (Fig. 1f). Furthermore, western blotting confirmed that smgGDS expression was reduced in vivo and in vitro after CDDP treatment (Fig. 1g, h). Additionally, the human-derived cell line HK-2 was evaluated to determine the clinical translational significance of this study; smgGDS was downregulated in HK-2 cells following CDDP treatment (Fig. S1b). Therefore, smgGDS was involved in CDDP-AKI and might have played a vital role in this process.

Genetic knockdown of smgGDS promoted CDDP-AKI

To explore the effect of smgGDS in CDDP-AKI, the *smgGDS*$^{+/-}$ (*KD*) mice used to establish the animal model for the smgGDS-knockout (*smgGDS*$^{-/-}$) mice were embryo-lethal (Fig. S1c–e)[19]. Furthermore, age- and sex-matched wildtype (WT) and *KD* mice were treated with CDDP (i.p.) for 72 h to establish the AKI model. Subsequently, the body and kidney weights were measured, and the kidney and blood samples were collected. After CDDP injection in the WT group, the kidney was swollen, the renal cortex was relatively ischemic (Fig. 2a, b Fig. S2a). Notably, these pathological manifestations presented as swelling and vacuolation of renal tubular epithelial cells with a tubular pattern (Fig. 2c). Comparatively, in *KD* mice, the renal injury was more severe and was mainly localized in the renal tubular cortex. Additionally, compared with that in WT mice, in *KD* mice, the whole kidney showed ischemia and swelling (Fig. 2a), the body weight decreased while the kidney/body weight ratio increased (Fig. 2b), and a large number of tubular patterns appeared with the renal tubular lumen significantly dilated, the renal tubular epithelial cells were swollen and detached, and the kidney injury score was increased (Fig. 2c, d). Moreover, SCr and BUN levels were markedly increased in the *KD* group compared with those in the WT group, suggesting a sharp decline in renal function in *KD* mice after CDDP-AKI compared with that in WT mice (Fig. 2e, f). Furthermore, regarding NGAL and KIM-1, the biomarkers of renal damage, NGAL was detected through immunohistochemistry and western blotting, while KIM-1 was detected using western blotting. Their expressions were increased in *KD* mice compared to WT mice after CDDP-AKI (Fig. 2c, g).

KD mice were more susceptible to CDDP and had more severe renal injury than WT mice. smgGDS insufficiency in mice resulted in higher levels of renal injury markers, such as BUN, SCr, and NGAL, and a considerable loss of renal tubular function compared with those in WT mice, suggesting that smgGDS might have played a protective role in CDDP-AKI.

PERK might be involved in the smgGDS-meditated CDDP-AKI process

The smgGDS-knockdown cell line was established to explore the underlying mechanism of CDDP-AKI, and shRNA targeting smgGDS produced a robust knockdown of smgGDS protein expression compared with control shRNA. For further mechanistic studies, a series of examination was designed (Fig. 3a), and RNA-seq was performed to explore the differentially expressed genes between the NC + CDDP and KD + CDDP groups.

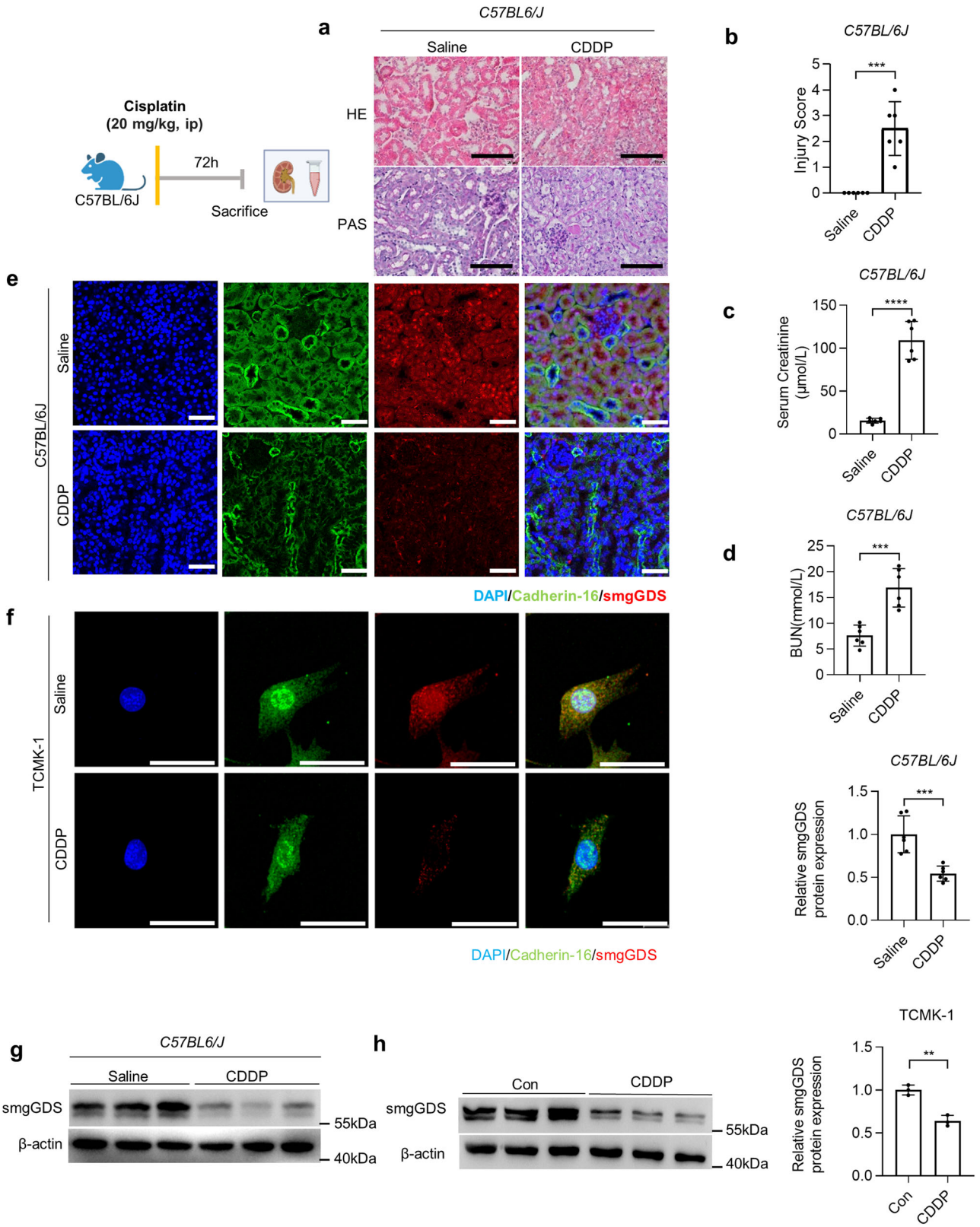

Fig. 1 | SmgGDS decreased in CDDP-AKI. a The HE and PAS staining of C57BL/6 J mice kidney treated with saline or cisplatin (scale bar: 50 μm); (**b**) the kidney injury score of C57BL/6 J mice kidney treated with saline or cisplatin; (**c**, **d**) serum creatinine and blood urea nitrogen determined at 72 h after CDDP or saline injection in C57BL6/J mice; (**e**) immunofluorescence staining of smgGDS (red) and cadherin-16 (green) in the kidney cortex of C57BL/6 J mice treated with saline or CDDP for 72 h (magnification: ×400, scale bar: 50 μm); (**f**) immunofluorescence staining of smgGDS (red) and cadherin-16 (green) in TCMK-1 treated with CDDP or saline (control group) (magnification: ×1000, scale bar: 50 μm); (**g**, **h**) western blot of smgGDS in kidney (n = 6) and TCMK-1 (n = 3) protein expression treated with saline or CDDP and quantified by ImageJ. CDDP, cisplatin; TCMK-1, mouse renal tubular epithelial cells; DAPI, nuclei; smgGDS, small GTP-binding protein GDP dissociation stimulator. All data presented are the means ± SD. $^{*}P < 0.05$, $^{**}P < 0.01$, $^{***}P < 0.001$, $^{****}P < 0.0001$.

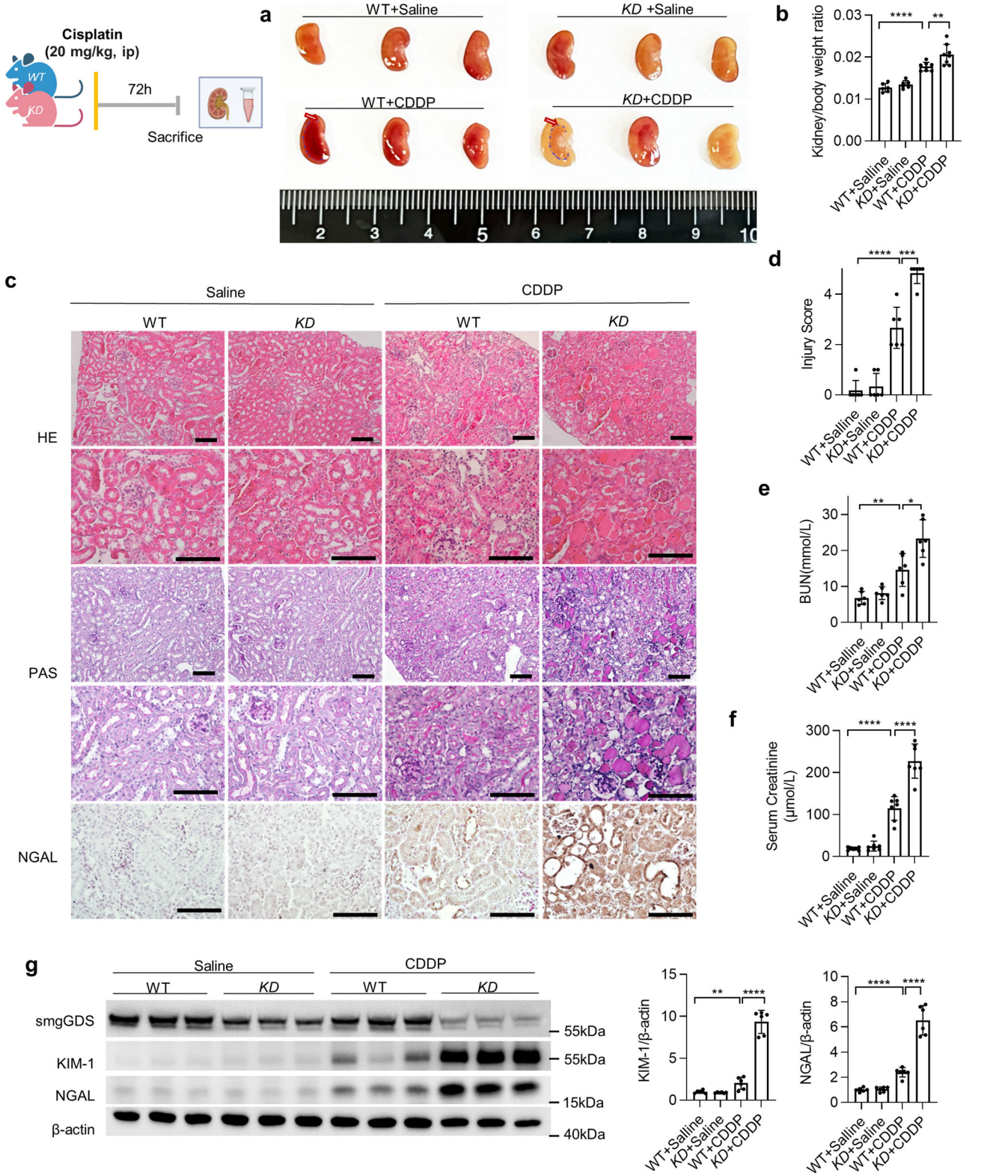

Fig. 2 | SmgGDS insufficiency promoted the cisplatin-induced AKI. a Coronal sections of the kidney from WT and *KD* mice injected with CDDP or saline intraperitoneally for 72 h; (**b**) the ratio of kidney and body weight (n = 6); (**c**) representative images of HE, PAS, and immunohistochemistry staining of NGAL of kidneys collected from WT and *KD* mice injected with CDDP or saline intraperitoneally for 72 h (magnification: ×200 HE and PAS upper panel, scale bar: 50 μm; ×400 HE, PAS and immunohistochemistry staining of NGAL lower panel, scale bar: 50 μm); (**d**) the injury score was evaluated as described in "Methods" (n = 6); (**e**, **f**) serum creatinine and blood urea nitrogen determined at 72 h after CDDP or saline injection (n = 6); (**g**) western blot KIM-1 and NGAL protein expression in the kidney collected from WT and *KD* mice injected with CDDP or saline and quantified by ImageJ (n = 6). WT wildtype, KD *smgGDS*$^{+/-}$, CDDP cisplatin, HE hematoxylin–eosin staining, PAS periodic acid–Schiff staining, DAPI nuclei, smgGDS small GTP-binding protein GDP dissociation stimulator, NGAL neutrophil gelatinase-associated lipocalin, KIM-1 kidney injury molecule 1. All data presented are the means ± SD. *$P < 0.05$, **$P < 0.01$, ***$P < 0.001$, ****$P < 0.0001$.

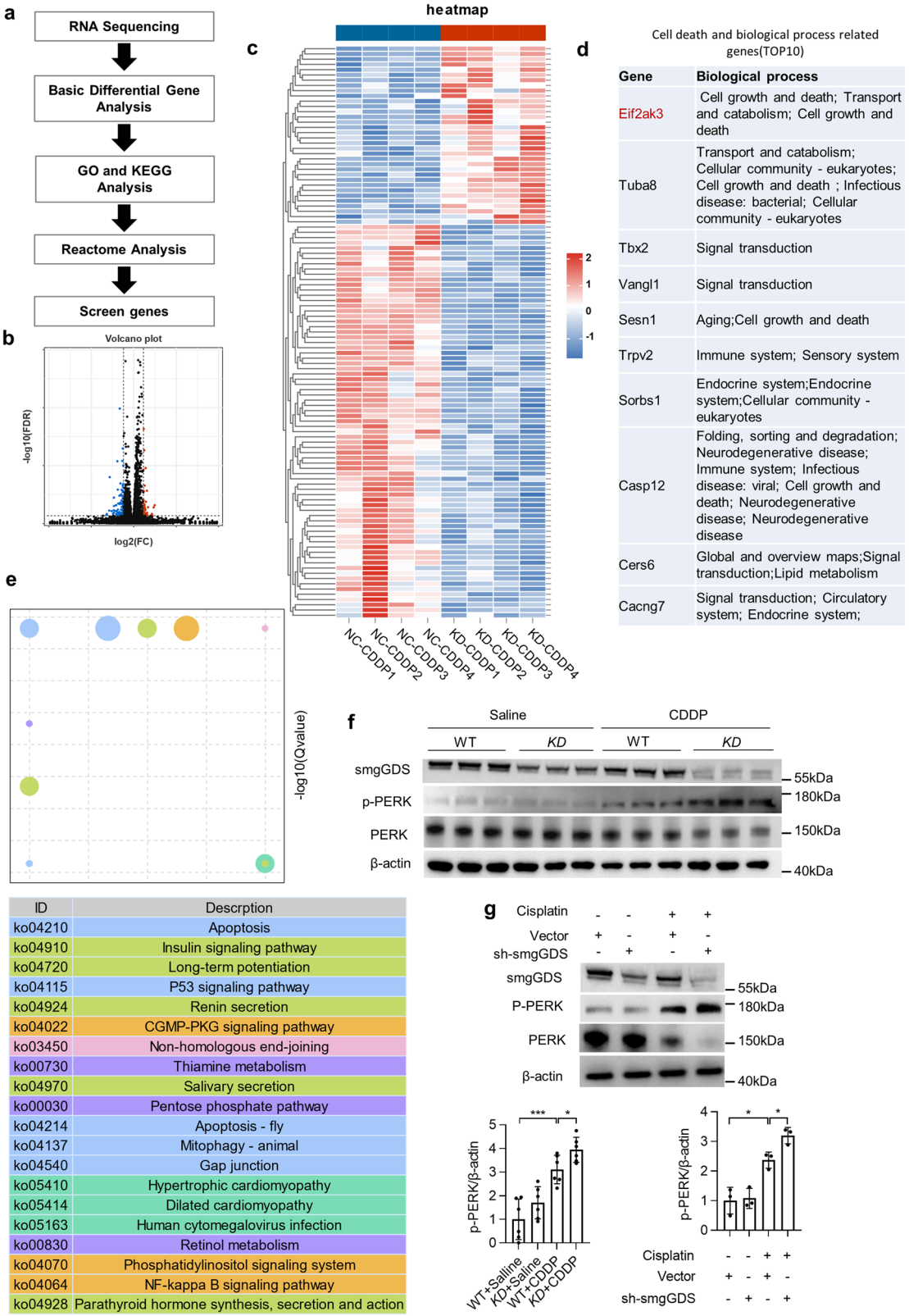

Gene	Biological process
Eif2ak3	Cell growth and death; Transport and catabolism; Cell growth and death
Tuba8	Transport and catabolism; Cellular community - eukaryotes; Cell growth and death ; Infectious disease: bacterial; Cellular community - eukaryotes
Tbx2	Signal transduction
Vangl1	Signal transduction
Sesn1	Aging;Cell growth and death
Trpv2	Immune system; Sensory system
Sorbs1	Endocrine system;Endocrine system;Cellular community - eukaryotes
Casp12	Folding, sorting and degradation; Neurodegenerative disease; Immune system; Infectious disease: viral; Cell growth and death; Neurodegenerative disease; Neurodegenerative disease
Cers6	Global and overview maps;Signal transduction;Lipid metabolism
Cacng7	Signal transduction; Circulatory system; Endocrine system;

ID	Descrption
ko04210	Apoptosis
ko04910	Insulin signaling pathway
ko04720	Long-term potentiation
ko04115	P53 signaling pathway
ko04924	Renin secretion
ko04022	CGMP-PKG signaling pathway
ko03450	Non-homologous end-joining
ko00730	Thiamine metabolism
ko04970	Salivary secretion
ko00030	Pentose phosphate pathway
ko04214	Apoptosis - fly
ko04137	Mitophagy - animal
ko04540	Gap junction
ko05410	Hypertrophic cardiomyopathy
ko05414	Dilated cardiomyopathy
ko05163	Human cytomegalovirus infection
ko00830	Retinol metabolism
ko04070	Phosphatidylinositol signaling system
ko04064	NF-kappa B signaling pathway
ko04928	Parathyroid hormone synthesis, secretion and action

Fig. 3 | PERK involved in smgGDS-mediated CDDP-AKI process. Transcriptome sequencing analysis of vector and smgGDS-knockdown TCMK-1 treated with CDDP (NC + CDDP vs. KD + CDDP). **a** Scheme of RNA-seq and bioinformatics analysis to screen the effector molecule of smgGDS knockdown; a volcano plot (**b**) and heat map (**c**) of different genes compared with NC + CDDP with KD + CDDP ($n = 4$, $Log_2^{(fold\ change)} \geq 1.5$, $P < 0.05$); (**d**) TOP10 genes related with the cell death and biological process of smgGDS knockdown affected in the CDDP-AKI; (**e**) KEGG analysis of top 20 pathways; (**f**) protein expression of PERK and p-PERK in vivo quantified by ImageJ ($n = 6$); (**g**) protein expression of PERK and p-PERK in vitro quantified by ImageJ ($n = 3$). WT wildtype, KD *smgGDS*$^{+/-}$, CDDP cisplatin, smgGDS small GTP-binding protein GDP dissociation stimulator, KEGG Kyoto Encyclopedia of Genes and Genomes. All data presented are the means ± SD. $^{*}P < 0.05$, $^{**}P < 0.01$, $^{***}P < 0.001$, $^{****}P < 0.0001$.

As expected, smgGDS insufficiency profoundly affected mRNA expression profiles (Fig. 3b, c). Next, bioinformatics analysis of the differentially expressed genes was performed (Fig. 3d, e, Fig. S2b, c). Gene Ontology (GO) analysis demonstrated that smgGDS insufficiency in CDDP-induced injury was related to molecular function, specialized in binding and catalytic activity, consistent with our expectation (Fig. S2b). A pathway analysis using the Kyoto Encyclopedia of Genes and Genomes (KEGG) database revealed that smgGDS promoted CDDP-induced injury through apoptosis (Fig. 3c). Furthermore, a Reactome analysis was performed to screen out the central aspects of smgGDS affecting apoptosis, which showed that PERK/eIF2α might be involved in the process (Fig. S2c). Combined with the heat map displaying differentially expressed genes in cellular processes and signal transduction, *EIF2A3K*, the PERK gene, was significantly influenced by smgGDS knockdown in CDDP-induced TCMK-1 injury (Fig. 3d).

The expression of the selected genes from RNA-seq (including *EIF2AK3*), which participated in cell processes and smgGDS function-related small GTPases (including *Rap1a*, *Rap1b*, *Rac1*, *Rab7*, and *Cdc42*), was validated by qPCR (Fig. S3a). Combined with the Reactome analysis, these analyses indicated that the mRNA expression level of *EIF2AK3* showed the most significant change, PERK, the *EIF2AK3*-translated protein, is suggested to be involved in downstream signaling. PERK phosphorylation level was detected using western blotting, which showed that p-PERK was increased in CDDP-AKI in *KD* mice compared with that in WT mice (Fig. 3f). In tubular epithelial cells, which undertake the major function of the kidney, p-PERK was markedly increased in KD treated with CDDP compared with that in NC (Fig. 3g). Interestingly, mRNA and protein expression were decreased, and the PERK phosphorylation level was relatively increased. We suspected that excessive PERK phosphorylation would consume PERK and have negative feedback on the transcription process; this phenomenon has been reported in some acute injuries[27]. However, the underlying mechanism needed further exploration.

Lastly, smgGDS knockdown accelerated CDDP-AKI, possibly mediated by PERK. As PERK is the central component of MAM-related ER stress, we suspected that smgGDS knockdown induced CDDP-induced kidney dysfunction via PERK, leading to ER stress.

smgGDS knockdown enhanced mitochondria-dependent apoptosis in CDDP-AKI in vivo and in vitro

KEGG analysis showed that apoptosis might be a crucial molecular outcome in CDDP-AKI. Additionally, a severe imbalance of ER homeostasis combined with PERK activation might modulate mitochondrial metabolism, and the key molecules involved in mitochondria-dependent apoptosis were detected[28]. Cleaved Caspase-3 was increased in *KD* mice treated with CDDP compared with those in WT mice (Fig. 4a). Furthermore, the function of Bcl-2 and BAX are tightly associated with mitochondria-dependent apoptosis. Bcl-2 decreased and BAX increased in CDDP-AKI *KD* mice compared with those in WT mice (Fig. 4a). Similar trends were observed in vitro (Fig. 4b). Terminal deoxynucleotidyl transferase-mediated dUTP nick-end labeling (TUNEL) assay and flow cytometry were performed to measure the apoptosis rate. In the kidneys of saline-injected mice, few TUNEL-positive cells were detected in WT and *KD* mice. Furthermore, high numbers of TUNEL-labeled cells were observed in the kidneys of WT and *KD* with CDDP-AKI, and apoptosis was markedly higher in *KD* mice than in WT mice (Fig. 4c). Additionally, the apoptosis rate of TCMK-1 was augmented by CDDP, which was exacerbated by smgGDS insufficiency (Fig. 4d). Overall, smgGDS might enhance mitochondria-dependent apoptosis in CDDP-AKI.

smgGDS insufficiency aggravated ER stress in CDDP-AKI in vivo and in vitro

PERK links the ER and mitochondria to react to various stresses and damage. Furthermore, PERK activation by UPR accumulation in the lumen of the ER leads to eIF2α subunit phosphorylation and inhibits translation[29]. We first observed an elevated eIF2α phosphorylation level in the kidneys of WT mice with CDDP-AKI and later discovered that this level was even more elevated in *KD* mice than in WT mice (Fig. 5a). And in the CDDP treated TCMK-1, eIF2α phosphorylation level of the KD group was increased compared with the NC group (Fig. 5b). eIF2α phosphorylation is a key switch for controlling global transcriptional levels because it makes eIF2β inactive, thereby causing a low transcriptional level[30]. Combining the mechanism mentioned above with the low transcript levels and high PERK phosphorylation levels after CDDP intervention in smgGDS-deficient cells and tissues, we propose that CDDP intervention after smgGDS knockdown increases PERK phosphorylation levels, which in turn activates eIF2α. In contrast, hyperphosphorylation of PERK might trigger a corresponding negative feedback mechanism that reduces PERK translation.

ER stress was detected in vivo and in vitro. We verified that GRP78, ATF4, and CHOP levels were increased in the kidney in vivo and in vitro after CDDP administration (Fig. 5a). Moreover, smgGDS insufficiency further elevated GRP78, ATF4, and CHOP levels in CDDP-induced renal injury in vivo and in vitro (Fig. 5a, b). The subcellular structure was observed using TEM. In the WT + Saline and *KD* + Saline group, the massive ER (red) was surrounded the mitochondria, and in the *KD* + Saline group, there are few ER slightly dilated (yellow arrow) (Fig. 5c). Furthermore, a part of the ER was dilated and mitochondria were swollen in the kidneys of WT mice after administering CDDP (Fig. 5c). Furthermore, a part of the ER was dilated (yellow arrow) and mitochondria were swollen in the kidneys of WT mice after administering cisplatin. ER swelling and rupture resulted in noticeable vacuolization, and aberrant mitochondria were observed in the kidneys of CDDP-treated *KD* mice (Fig. 5c). As previously described, PERK is strongly associated with mitochondria and ER. However, the role of ER stress in the apoptosis resulting from smgGDS insufficiency in CDDP-AKI was not analyzed. The 4-PBA, a global ER stress inhibitor, was used in order to identify the link between apoptosis and ER stress resulting from smgGDS in CDDP-AKI. The results showed that 4-PBA could suppress ER stress induced apoptosis, compared with the NC and KD cells treated with CDDP (Fig. 6a), decrease the expression of Cleaved Caspase-3 and BAX, and increase Bcl-2 expression (Fig. 6b) and the decreased expression of p-PERK, GRP78, ATF4, and CHOP in the KD cells of the CDDP-AKI model treated with 4-PBA (Fig. 6b).

In summary, smgGDS insufficiency activated PERK, aggravated CDDP-induced ER stress and mitochondrial damage, eventually resulting in severe apoptosis and renal injury.

SmgGDS insufficiency increased apoptosis via PERK/eIF2α/CHOP axis

We have already identified that PERK might be involved in smgGDS deficiency-induced ER stress and apoptosis; however, the underlying mechanism requires further exploration. PERK and eIF2α phosphorylation were inhibited by PERKi and ISRIB, respectively, in TCMK-1. Furthermore, PERKi decreased p-PERK and p-eIF2α levels, and the eIF2α phosphorylation inhibitor (ISRIB) only decreased the level of p-eIF2α in the smgGDS-knockdown TCMK-1 treated with CDDP (Fig. 7a). Therefore, we suspected that PERK is upstream of eIF2α. Furthermore, we investigated the impact of PERKi on ER stress and apoptosis. SmgGDS knockdown-induced apoptosis and increased ER stress were reversed by PERKi injection, which was demonstrated by the increased Bcl-2 and decreased BAX and Cleaved Caspase-3 levels (Fig. 7b). Additionally, PERKi intervention markedly decreased the number of apoptotic cells (Fig. 7c). Compared with those in KD cells treated with CDDP, the ER stress-related components GRP78, ATF4, and CHOP decreased after PERKi treatment (Fig. 7b). Considering the changes in Caspase-3, Bcl-2, and BAX observed in this study, which indicated potential mitochondrial injury, the mitochondrial membrane potential was assessed using 5′,6,6′-tetrachloro-1,1′,3,3′-tetraethylbenzimidazolylcarbocyanine iodide (JC-1). After treated with cisplatin, NC cell the JC-1 monomers signal increased and the JC-1 aggregates signal decreased compared with treated with saline. Furthermore, in the KD cell line treated with cisplatin, the JC-1 aggregates significantly decreased compared with the JC-1 monomers significantly increased, compare with NC cell treated with cisplatin, suggested that the mitochondrial membrane

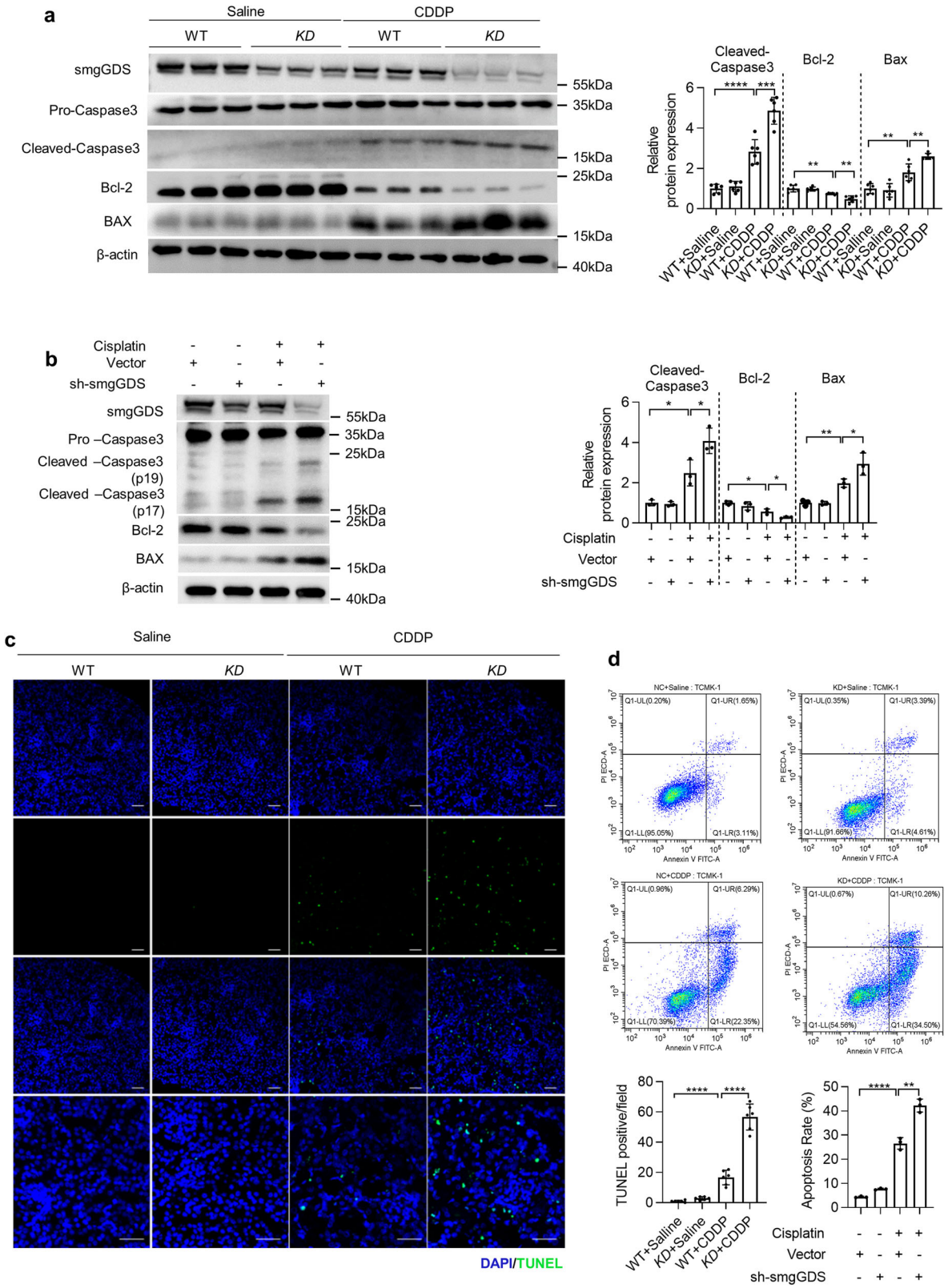

Fig. 4 | SmgGDS insufficiency enhanced mitochondria-dependent apoptosis in CDDP-AKI. a Western blot to detect the expression and activation of Caspase-3, PARP, Bcl-2, and BAX in the kidneys of WT and *KD* mice injected with CDDP or saline intraperitoneally for 72 h was quantified by ImageJ (n = 6); (**b**) western blot to detect the protein expression and activation of Caspase-3, Bcl-2, and BAX in TCMK-1 treated with CDDP or saline was quantified by ImageJ (n = 3); (**c**) representative images of apoptotic cells labeled by TUNEL in the kidney cortex of WT and *KD* mice injected with CDDP or saline intraperitoneally for 72 h, and the TUNEL-positive cells were counted as described in the "Methods" Section (scale bar: 50 μm). **d** Apoptosis detection by flow cytometry labeled with PI and Annexin V FITC in NC and KD TCMK-1 treated with CDDP or saline; CDDP cisplatin, NC control group of TCMK-1, KD knockdown of smgGDS in TCMK-1, WT wildtype, *KD smgGDS*$^{+/-}$, TUNEL terminal deoxynucleotidyl transferase-mediated dUTP nick-end labeling; smgGDS, small GTP-binding protein GDP dissociation stimulator. All data presented are the means ± SD. *$P < 0.05$, **$P < 0.01$, ***$P < 0.001$, ****$P < 0.0001$.

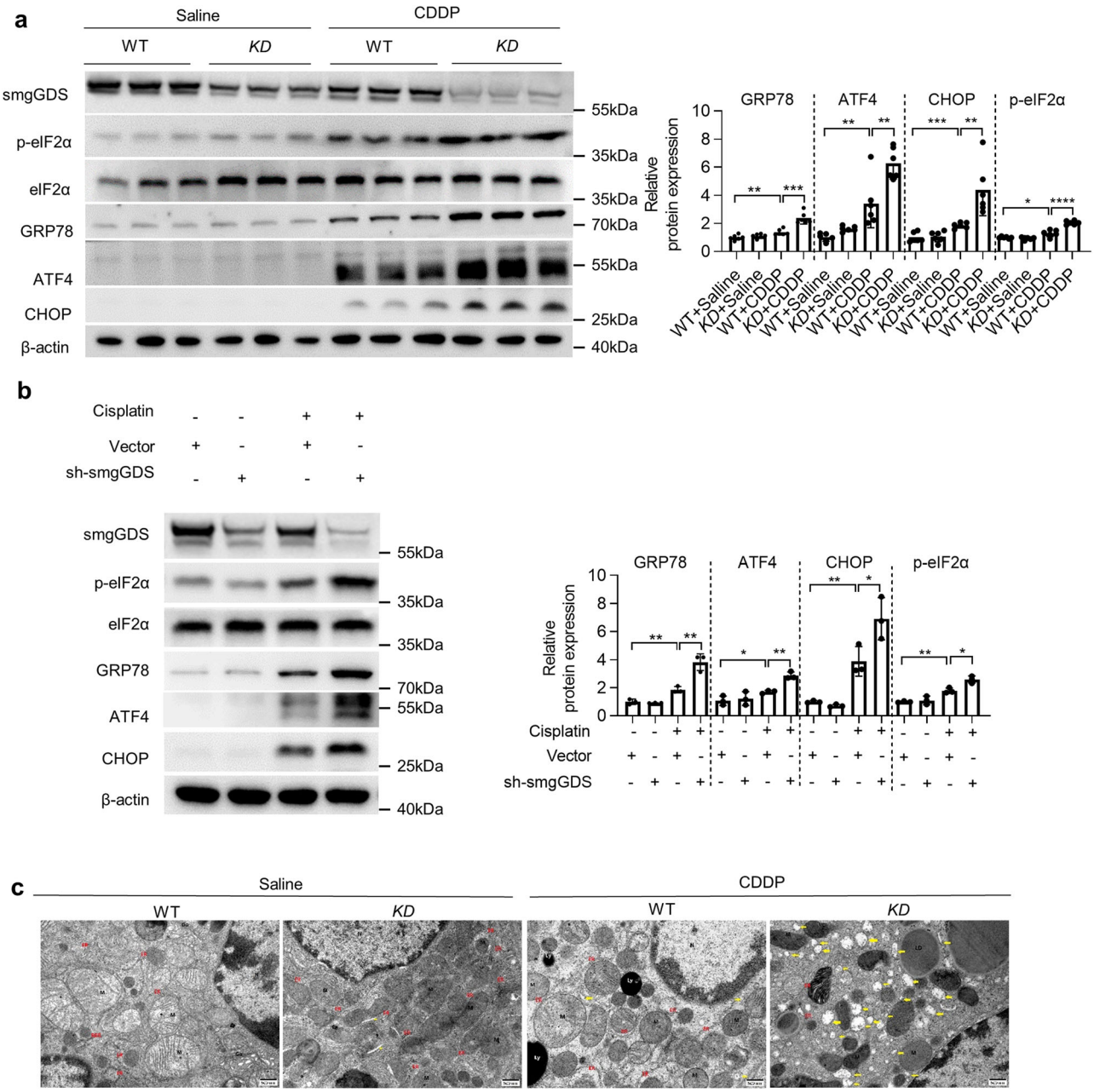

Fig. 5 | SmgGDS insufficiency aggravated endoplasmic reticulum stress in CDDP-AKI. a Western blot to detect the protein expression of eIF2α, p- eIF2α, GRP78, ATF4 and CHOP in the kidneys of WT and *KD* mice injected with CDDP or saline intraperitoneally for 72 h; (**b**) western blot to detect the protein expression of eIF2α, p- eIF2α, GRP78, ATF4 and CHOP in TCMK-1 treated with CDDP or saline; (**c**) transmission electron microscopy to observe the morphology of subcellular organelles in the kidneys of WT and *KD* mice injected with CDDP or saline (magnification: ×25.0 k, scale bar: 500 nm); WT wildtype, *KD smgGDS*$^{+/-}$, DAPI nuclei, CDDP cisplatin, smgGDS, small GTP-binding protein GDP dissociation stimulator. All data presented are the means ± SD. $^{*}P < 0.05$, $^{**}P < 0.01$, $^{***}P < 0.001$, $^{****}P < 0.0001$.

potential declined significantly. The result showed that smgGDS knockdown in cells exacerbated the mitochondrial membrane potential damage caused by CDDP compared to NC cells (Fig. 7d). To further clarify the link between PERK and mitochondria function, the PERKi was utilized in KD cells treated with CDDP. It showed that the PERKi treatment mitigated the smgGDS knockdown induced mitochondrial membrane potential declined (Fig. 7d). These findings suggested that smgGDS-knockdown-induced ER stress and mitochondria related apoptosis can be reversed by inhibiting PERK phosphorylation. PERK has been proposed to be crucial for mediating smgGDS-induced apoptosis and ER stress.

In order to clarify role of smgGDS within CDDP-AKI, the smgGDS overexpression cell line was established. Firstly, the results showed that the overexpression of smgGDS could reduce the cell apoptosis ratio (Fig. 8a) and decrease the expression of Cleaved Caspase-3 and BAX, while increasing the expression of Bcl-2 (Fig. 8b). Furthermore, compared with the OE-NC CDDP-treated group, the smgGDS overexpression cells showed decreased p-PERK levels (Fig. 8c). Furthermore, the overexpression of smgGDS could reduce the expression of GRP78, ATF4, and CHOP in the cells treated with CDDP (Fig. 8c). The CCT020312, a PERK phosphorylation agonist, was used, revealing that the activation of PERK could reverse the protective effect of smgGDS overexpression (Fig. 8a–c).

Interestingly, although the protein levels of pro-PERK decreased after smgGDS knockdown after CDDP intervention, they increased following the use of PERKi and ISRIB and activation of PERK by CCT020312

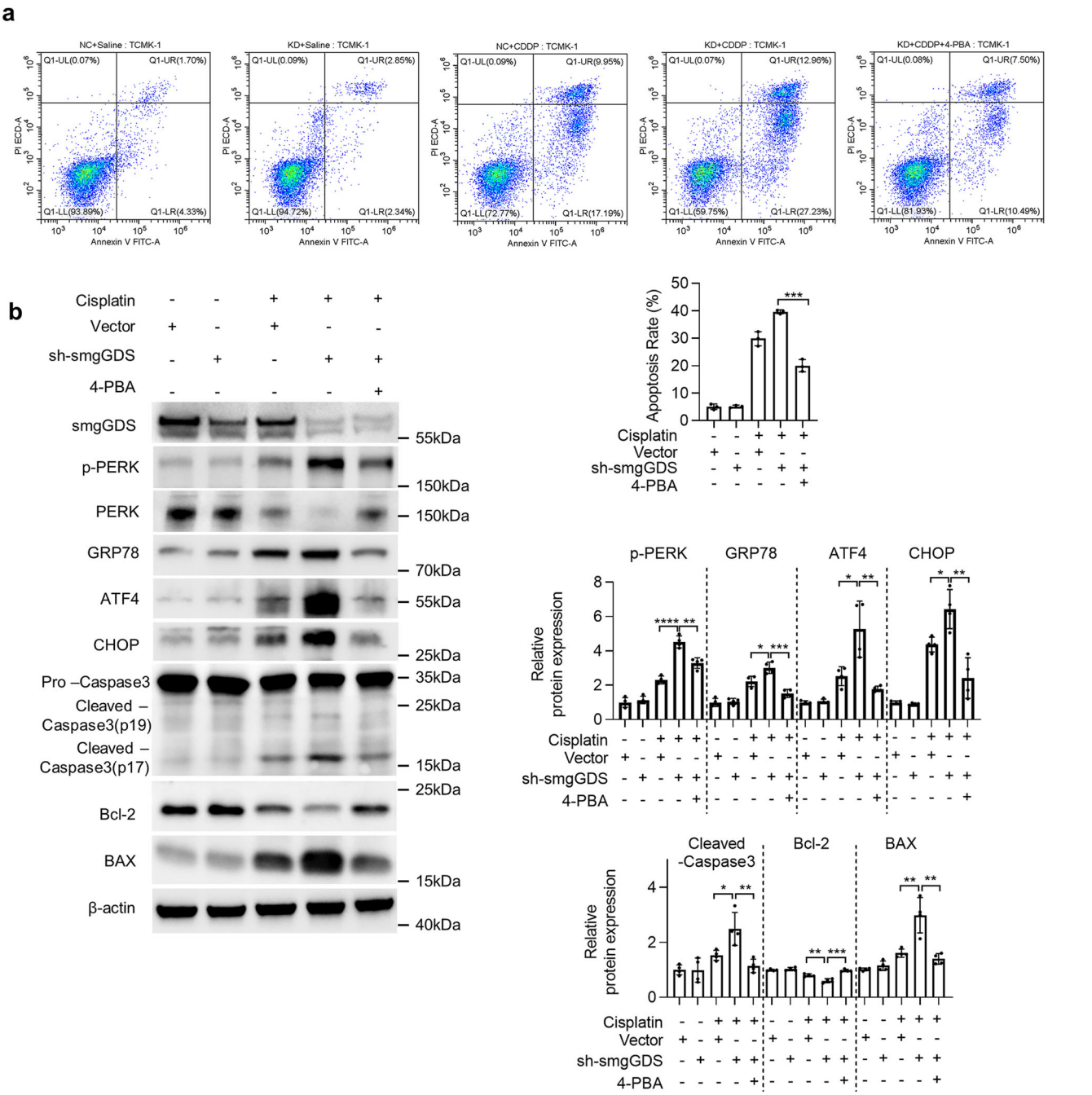

Fig. 6 | Suppressed of endoplasmic reticulum stress reduced apoptosis in CDDP-induced AKI. a Apoptosis detected by flow cytometry labeled with PI and Annexin V FITC in NC and KD TCMK-1 treated with CDDP or saline and/or 4-PBA; (**b**) western blot to detect the influence of 4-PBA to the protein expression of smgGDS, p-PERK, PERK, GRP78, ATF4, CHOP, Cleaved-Caspase3, Pro-Caspase3, Bcl-2, and BAX in NC and KD TCMK-1 treated with CDDP or saline; 4-PBA 4-phenylbutyric acid, CDDP cisplatin, smgGDS small GTP-binding protein GDP dissociation stimulator. All data presented are the means ± SD. $^{*}P < 0.05$, $^{**}P < 0.01$, $^{***}P < 0.001$, $^{****}P < 0.0001$.

also decreased pro-PERK protein levels (Figs. 6a, 8c). Combined with the finding from earlier research that eIF2α activation suppresses levels across the board during transcription, this finding raises the possibility that elevated PERK phosphorylation depletes pro-PERK and activates eIF2α, resulting in decreased PERK transcript levels and, ultimately, a significant decrease in pro-PERK protein levels. We confirmed this hypothesis by examining the transcription levels of the related molecules (Fig. S3b). The inhibition of eIF2α phosphorylation resulted in significantly higher transcript levels of PERK and eIF2α, which were much higher than those in the control group. This finding suggests that phosphorylation of eIF2α is the primary factor causing the downregulation of PERK transcript levels and that it is a key molecule that controls transcription throughout the organism.

Discussion

This study demonstrates that smgGDS contributes to CDDP-induced kidney damage, which to the best of our knowledge, has not been reported previously. The contributions of this study include the following. First, we found that smgGDS was significantly downregulated in CDDP-AKI in vivo and in vitro and that the decrease in smgGDS expression was predominantly located in renal tubular epithelial cells. Second, after smgGDS knockdown, PERK phosphorylation was increased in CDDP-AKI, which activated the

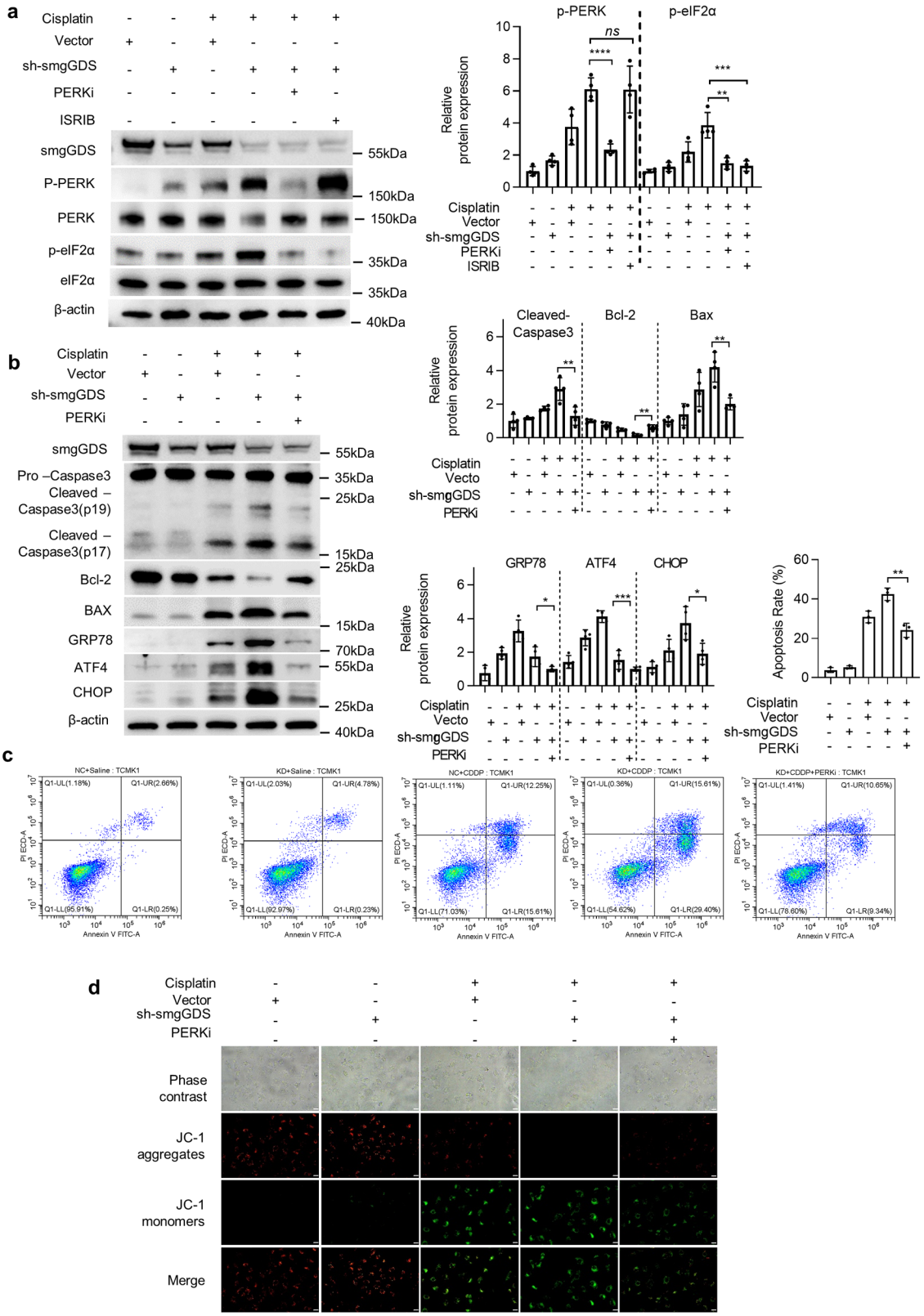

Fig. 7 | SmgGDS insufficiency increased apoptosis via PERK-dependent ER stress. a The protein expression and phosphorylation of PERK and eIF2α in CDDP or saline-treated TCMK-1 treated with PERKi (5 nM) or ISRIB (25 nM); (**b**) the protein expression and activation related to apoptosis including Caspase-3, Bcl-2, BAX, GRP78, ATF4, and CHOP normalized by β-actin in CDDP or saline-treated TCMK-1 treated with PERKi (5 nM); (**c**) apoptosis detected by flow cytometry labeled by PI and Annexin V FITC in CDDP or saline-treated NC and KD TCMK-1 treated with PERKi (5 nM); (**d**) the mitochondria membrane potential detection in CDDP or saline-treated NC and KD TCMK-1 treated with PERKi (5 nM, scale bar: 20 μm). CDDP cisplatin, PERKi selective PERK phosphorylation inhibitor, smgGDS small GTP-binding protein GDP dissociation stimulator, JC-1 mitochondrial membrane potential probe. All data presented are the means ± SD. $^{*}P < 0.05$, $^{**}P < 0.01$, $^{***}P < 0.001$, $^{****}P < 0.0001$.

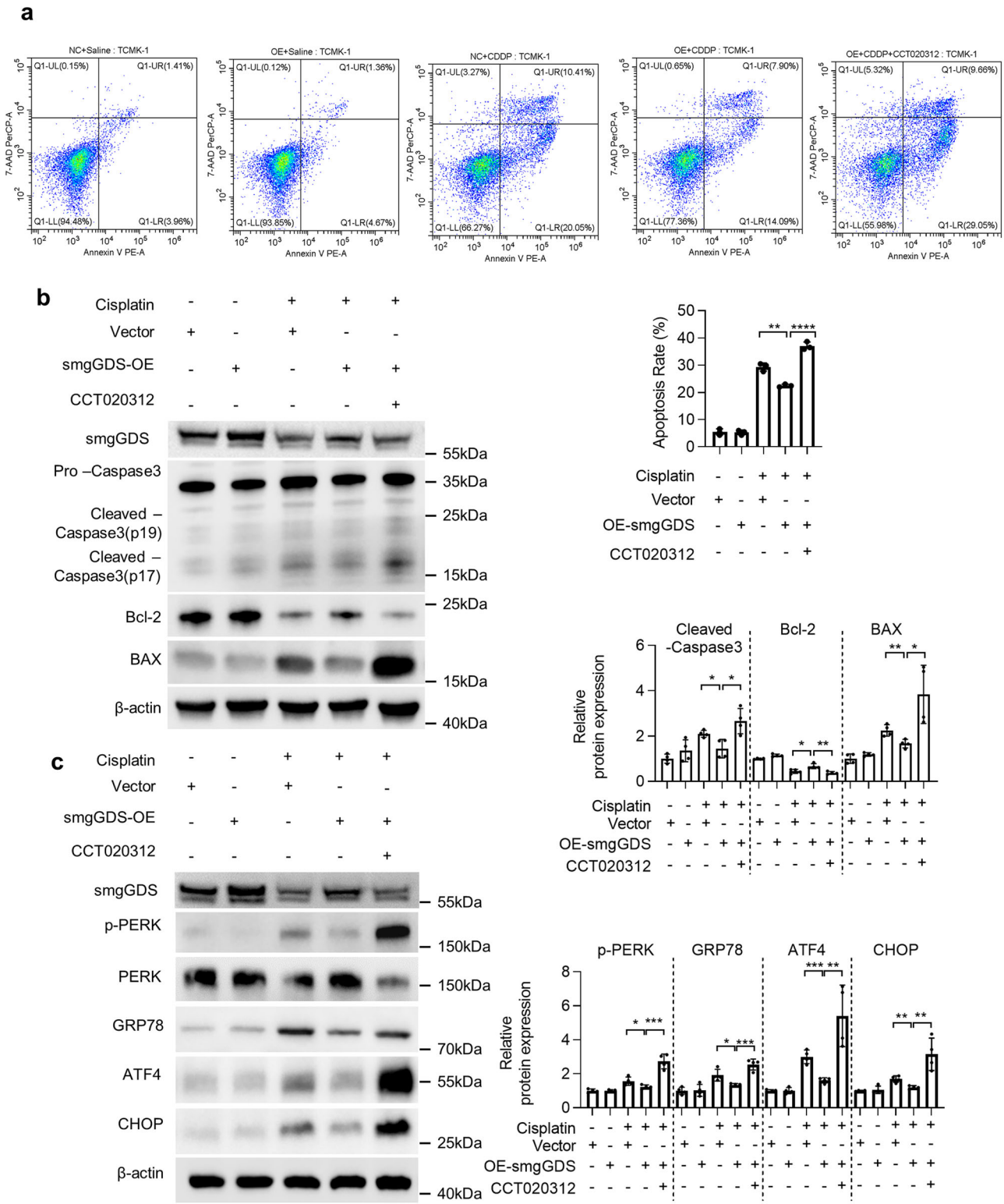

Fig. 8 | SmgGDS overexpression alleviated CDDP-induced apoptosis via PERK-dependent ER stress. a Apoptosis detected by flow cytometry labeled by 7-AAD and Annexin V PE in CDDP or saline-treated OE-NC and OE TCMK-1 treated with CCT020312 (10 μM); (**b**) the protein expression and activation related to apoptosis including smgGDS, Caspase-3, Bcl-2, and BAX normalized by β-actin in CDDP or saline-treated OE-NC and OE TCMK-1 treated with CCT020312 (10 μM); (**c**) the protein expression including smgGDS, GRP78, ATF4, and CHOP normalized by β-actin in CDDP or saline-treated OE-NC and OE TCMK-1 treated with CCT020312 (10 μM). CDDP, cisplatin; CCT020312, PERK phosphorylation agonist; OE overexpression of smgGDS in TCMK-1, smgGDS small GTP-binding protein GDP dissociation stimulator. All data presented are the means ± SD. $^{*}P < 0.05$, $^{**}P < 0.01$, $^{***}P < 0.001$, $^{****}P < 0.0001$.

PERK/eIF2α/CHOP axis and increased ER stress. And the smgGDS insufficiency induced ER stress and apoptosis could be reverse by ER stress inhibitor. Lastly, the inhibition of PERK phosphorylation ameliorated CDDP-AKI caused by smgGDS knockdown and reversed the detrimental effect of smgGDS knockdown on ER stress, while overexpression of smgGDS mitigated ER stress and apoptosis. Moreover, to the best of our knowledge, this is the first study to demonstrate that smgGDS modulates ER stress and apoptosis via the PERK/eIF2α/CHOP pathway in CDDP-AKI.

Nephrotoxicity is the major side effect of CDDP, which would cause irreversible damage in patients with malignant tumors[31]. Statins could relieve CDDP-induced side effects, including hearing loss and renal injury, and smgGDS has been reported to be a vital mediator of statins' pleiotropic effects as previous metioned. However, studies on the role of smgGDS in human diseases are limited, and to the best of our knowledge, there has been no research on smgGDS function in kidneys. In our study, we found, for the first time, to the best of our knowledge, that smgGDS was expressed in kidneys that and smgGDS was downregulated in CDDP-AKI. Since embryonic lethality resulted from the systemic knockout of smgGDS in mice, smgGDS global knockdown mice were established. SmgGDS knockdown greatly aggravated CDDP-AKI, which manifested as a marked increase in renal tubular epithelial cell death, loss of tubular function, appearance of numerous tubular patterns, and severe kidney cortex ischemia. These findings provide the first convincing evidence that smgGDS might play a protective role in renal injury.

The KEGG analysis of RNA-Seq data implied that apoptosis might be the major form of cell death in smgGDS deficiency-induced CDDP-AKI. To confirm this result, the cell apoptosis ratio and apoptosis biomarkers, such as Caspase-3, Bcl-2, and Bax, were detected in vivo and *vitro*. We confirmed that smgGDS deficiency-induced renal epithelial cell death via apoptosis, but the specific mechanism was unclear. Through sequencing the transcriptome, we identified significant alterations in *EIF2AK3*, the ER stress kinase PERK gene, indicating that PERK might be a key mediator of CDDP-AKI exacerbated by smgGDS knockdown. PERK is an ER stress sensor, and its increased phosphorylation activates eIF2α, resulting in an overall downregulation of transcriptional levels and increased transcriptional levels of stress-related molecules, including ATF4 and CHOP[32]. Following smgGDS knockdown, p-PERK levels were markedly increased in the CDDP-AKI model. Under ER stress, the distance between the ER and mitochondria is shortened, reactive oxygen species produced by ER stress can be transferred to mitochondria, and CHOP promotes the transcriptional upregulation of mitochondrial apoptosis-related genes, such as *BAX*, causing MAM-related apoptosis. It was reported that use of the ER stress inhibitor 4-PBA not only inhibited ER stress but also improved mitochondrial morphology and inhibited mitochondrial pathway-dependent apoptosis, suggesting a close relationship between the mitochondria and ER[33–36]. Moreover, in the smgGDS knockdown cells, 4-PBA supplementation reversed the ER stress and apoptosis in cells treated with CDDP. These results demonstrated that the apoptosis caused by smgGDS insufficiency was tightly associated with ER stress and PERK might be a key molecular player.

The TEM showed that the ER lumen was significantly expanded, and the mitochondria were swollen, increasing their size. The ER stress-related PERK downstream molecules, including ATF4 and CHOP, increased after smgGDS knockdown in CDDP-AKI, and GRP78 showed the same trends. Above all, we suspected that smgGDS insufficiency in CDDP-AKI activated PERK, which, in turn, led to the initiation of ER stress and activated the apoptotic pathway via MAMs, finally resulting in cell death.

The ER is the organelle primarily responsible for protein modification, quality control, and transport[37,38]. smgGDS was believed to primarily control the activity of partial small GTPases from the Ras, Rho, and Rap families, facilitating GDP/GTP exchange. However, more recent research has revealed that smgGDS is important for the post-translational modification and transport of small GTPases, and its absence can hamper these activities, leading to the accumulation of unmodified proteins in the ER[39]. SmgGDS comprises two spliceosomes, smgGDS-607 and smgGDS-558[40]. Variations in the ratio of these spliceosomes influence prenylation modifications of small GTPases[39]. Additionally, smgGDS facilitates the transport of associated proteins between the nucleus, plasma membrane, and inner membrane. Furthermore, smgGDS might use its N-terminal nuclear export sequence to return small GTPases to the cytoplasm when nuclear signaling is complete[41]. On completing prenylation processing in ER, smgGDS likely functions as a chaperone to assist the small GTPase of prenylation in moving to the plasma membrane or other cell regions[42]. Additionally, the detection of PERK downstream molecules revealed that smgGDS knockdown caused markedly increased GRP78, ATF4, and CHOP expression in the CDDP-AKI model. Furthermore, observing ER morphology using TEM revealed that after administering CDDP to the *KD* mice, the ER of the renal cortex was significantly dilated, and a large number of vacuoles appeared. Lastly, the overexpression of smgGDS could decrease the expression of GRP78, ATF4, and CHOP in cells treated with CDDP. In conclusion, in CDDP-AKI, smgGDS is likely involved in maintaining ER homeostasis and assisting in protein transport, modification, and degradation; therefore, its insufficiency impairs related protein post-translational modification and increases unfolded or misfolded protein accumulation in the ER and PERK activation leading to severe ER stress; while the overexpression of smgGDS helps the ER in maintaining normal function to resist external stress.

Interestingly, in our study, although the protein levels of prototypical PERK and PERK mRNA level significantly decreased after smgGDS knockdown and PERK activation, PERK mRNA level increased with the promoting PERK and eIF2a phosphorylation. This raises the hypothesis that high PERK phosphorylation depletes prototypical PERK and activates eIF2α, resulting in lower PERK transcript levels and a substantial decrease in prototypical PERK protein. We tested the validity of this theory by investigating the transcription levels of linked molecules. We discovered that reducing eIF2α phosphorylation considerably increased the mRNA levels of PERK and eIF2α compared with those in the control group. Eukaryotic cells have evolved a UPR to restore ER homeostasis in response to an imbalance in protein folding capacity[43]. The inhibition of PERK phosphorylation can effectively reduce CHOP expression and ER-associated reactive oxygen species production[44]. A negative feedback mechanism exists in the PERK/eIF2α/CHOP axis, where overexpression of CHOP leads to increased dephosphorylation of eIF2α, restoring global translation that is inhibited in the ER stress state[45]. Above all, we suspected that the inhibition of eIF2α led to an increase in PERK transcription and translation due to negative feedback but did not inhibit PERK phosphorylation. PERK was still activated, and ER stress was still initiated; hence, cell damage was not reduced. The inhibition of PERK turned off ER stress receptors and reduced ER stress, which, in turn, led to a reduction in MAM-related apoptosis.

This study suggests that eIF2α phosphorylation is the principal mechanism responsible for the downregulation of PERK transcription levels and is a critical transcription-regulating molecule in the entire organism. However, it is the activation of PERK that is central to the ER stress and MAM-related apoptosis caused by smgGDS deficiency. In other words, the ER stress and associated apoptotic phenotype caused by smgGDS insufficiency is PERK dependent.

There are some limitations in this study. First, this study focused solely on the effects of global smgGDS knockdown on CDDP-AKI. Given that smgGDS-607 and smgGDS-558 had various activities within cells and the influence of altered spliceosome ratios on disorders, such as tumors, it is possible that the change in the spliceosome ratio also affected CDDP-AKI, which was not considered in this study. Secondly, the effect of smgGDS on ER stress might be due to its role in the post-translational modification and transport of small GTPases, which require prenylation by smgGDS to properly anchor them to the plasma membrane. Additionally, smgGDS could help Rac1 transfer into the nucleus. The next stage of our research will be to elucidate the specific role of smgGDS by investigating the effect of its deletion on the intracellular location of small GTPases.

smgGDS shows potential as a molecule that can influence ER stress in CDDP-AKI, broadening our understanding of its biological function. Our study confirms that smgGDS knockdown exacerbates CDDP-AKI,

suggesting that smgGDS plays a role in kidney-related diseases. Based on these findings, smgGDS may be a biological target for diagnosing, preventing, and treating CDDP-AKI.

In conclusion, we determined the expression of smgGDS in kidneys for the first time to the best of our knowledge. Our findings indicate that smgGDS insufficiency aggravates CDDP-AKI and reveal the vital role of smgGDS in CDDP-AKI. Notably, in CDDP-AKI, smgGDS insufficiency activates PERK-dependent ER stress and accelerates MAM-related apoptosis. The study of smgGDS function in CDDP-AKI may provide a biomarker and improve our understanding of smgGDS in human disease.

Methods

Reagents

The following reagents were used in this study: Cisplatin (MedChemExpress, Shanghai, China), Zoletil®50 (Virbac, Carros, France), 4% paraformaldehyde universal tissue fixative (Biosharp, Hefei, China), hematoxylin–eosin (HE) kit (BaSO, Zhuhai, China), periodic acid–Schiff (PAS) kit (BaSO, Zhuhai, China), neutral balsam (Solarbio, Beijing, China), 100X citrate antigen retrieval solution (BBI, Shanghai, China), Triton X-100 (Solarbio), Normal Goat Serum (Solarbio), PageRuler Protein ladder (Thermo Fisher, Waltham, MA USA) RIPA buffer (NCM Biotech, Suzhou, China), sodium dodecyl sulfate-polyacrylamide gel electrophoresis (SDS-PAGE) loading buffer 5X (NCM Biotech, Suzhou, China), proteolytic protease and phosphatase inhibitor cocktail (NCM Biotech, Suzhou, China), TRIzol (Tiangen, Beijing, China), PrimeScript RT reagent Kit with gDNA Eraser (TAKARA, Kusatsu, Japan), TB Green Premix Ex Taq II (TAKARA, Kusatsu, Japan), 3,3'-diaminobenzidine tetrahydrochloride (DAB, ZSGB-Bio, Beijing, China), fetal bovine serum (FBS, Gibco, NY, CA, USA), Eagle's minimum essential medium (MEM, Hyclone, Logan, UT, USA), penicillin–streptomycin (Beyotime, Shanghai, China), PE Annexin V Apoptosis Detection Kit I (BD Bioscience, Franklin Lakes, NJ, USA), FITC Annexin V Apoptosis Detection Kit I (BD Bioscience, Franklin Lakes, NJ, USA), lentiviruses containing shRNA targeting mouse smgGDS-shRNA and control vectors with anti-puromycin (LV-shsmgGDS-Puro, LV-shNC-Puro, HanBio, Shanghai, China), polybrene (HanBio, Shanghai, China), lentiviruses containing smgGDS overexpression (OE) and empty vectors (LV-OE-smgGDS-ZsGreen-Puro, LV-ZsGreen-Puro, HanBio, Shanghai, China), 4-Phenylbutyric acid (4-PBA, MedChemExpress, Shanghai, China), GSK2606414 (selective PERK phosphorylation inhibitor [PERKi], MedChemExpress, Shanghai, China), and selective inhibitor of eIF2α/eIF2S1 Ser51 phosphorylation (ISRIB, Sigma-Aldrich, St. Louis, MO, USA), CCT020312 (selective PERK phosphorylation agonists, MedChemExpress, Shanghai, China). The antibodies for immunohistochemistry and primers used in this study are listed in Tables S1, S2.

Animals

C57BL/6 J mice (strain no. N000013) were purchased from GemPharmatech (Nanjing, China). Additionally, smgGDS hetero-deficient (*smgGDS*$^{+/-}$, strain n. T014825) C57BL/6 J background mice were obtained from GemPharmatech. The mice were raised in Specific Pathogen Free environment under the 12 h-light and 12 h-dark cycle. Subsequently, at 3–4 weeks, DNA was extracted from the mice tails. Next, WT and *KD* genes were amplified using their primers, and DNA agarose gel electrophoresis was performed to confirm the genotype. The procedure for genotype identification was performed, as described previously[46]. The data and primers are presented in Fig. S1d and Table S3.

The mice used in this study were male, aged 8–10 weeks, and weighed 22 ± 3 g. We established the CDDP-AKI model by administering a dosage of CDDP (20 mg/kg, i.p.) to mice, while a control group was given saline[47]. The mice were anesthetized with Zoletil®50 72 h after CDDP treatment, and then the samples were collected for the further study, after that the mice were euthanized using CO_2. The mouse carcasses were frozen and processed and were subsequently enclosed and delivered to Yangzhou University Animal Carcass Disposal Center for centralized harmless disposal. There were no surplus animals. All animal experiments were approved by the Ethics Committee of Yangzhou University (approval no. 202210006) and were conducted in accordance with the National Institutes of Health Guidelines for the Care and Use of Laboratory Animals.

Cell culture and in vitro treatment

TCMK-1 (normal mouse renal tubular epithelial cell line) was purchased from the American Type Culture Collection (Manassas, VA, USA) (#CCL-139) and cultured in MEM containing 10% fetal bovine serum (FBS) and 1% penicillin–streptomycin (AA) at 37 °C in a 5% CO_2 incubator. HK-2 (proximal renal tubular epithelial cell line derived from normal human) was obtained from the Chinese Academy of Sciences and cultured in DMED/F12 containing 10% FBS and 1% AA 37 °C in a 5% CO_2 incubator. Cells were transferred to a medium containing 1% FBS for 12 h for starvation. Then, TCMK-1 and HK-2 were treated with CDDP (20 μM) dissolved in saline, and the control group was treated with saline. Subsequently, the PERKi (5 nM), ISRIB (25 nM), 4-PBA (5 mM), and CCT020312 (5 μM) were used[48–50].

Lentiviral transfection

To obtain a stable smgGDS-knockdown and smgGDS-OE cell lines, transfected LV-smgGDS-Puro and LV-OE-smgGDS-ZsGreen-Puro cell lines were used as the KD and OE group, and transfected LV-shNC-Puro and LV-ZsGreen-Puro cell lines were used as the control group (NC and OE-NC) at multiplicity of infection = 1. The smgGDS-shRNA sequence Top strand: GATCCGTAGAGATCGTCCAACAGAACTCGAGTTCTG TTGGACGATCTCTATTTTTTG, Bottom strand:

AATTCAAAAAATAGAGATCGTCCAACAGAACTCGAGTTCTG TTGGACGATCTCTACG. The information of the plasmids, sh-smgGDS(225202) OE-smgGDS(225203), was submitted to Addgene. Twenty-four hours before lentiviral transfection, TCMK-1 was seeded into six-well plates. The next day, when the cell density was about 50%, the original medium was exchanged for a fresh medium supplemented with 6 μg/mL polybrene and LV-smgGDS-Puro and LV-NC-Puro (or LV-OE-smgGDS-ZsGreen-PURO and LV-ZsGreen-Puro) were added and incubated at 37 °C. Next, fresh medium was added into plates to dilute polybrene to half of initial concentration after 4 h and re-added after 24 h incubation. After transfection with lentivirus containing the anti-puromycin gene, medium added with puromycin (2 μg/mL) to select stable transfectants. The verification of transfection efficiency by western blotting is shown in Fig. 3g. Furthermore, the rescue assay was conducted to exclude the off-target interference shown in Fig. S3c, d.

Histological assessment

Mice kidney tissues were fixed in 4% paraformaldehyde, embedded in paraffin, and sequentially sectioned using a rotary microtome (LeicaBiosystems, Weztlar, Germany) to prepare paraffin sections (5 μm). Next, the sections were stained with HE and PAS kit and sealed with neutral balsam. The injury score was calculated as previously described[51]. Briefly, the histopathologic injury score was calculated using a single-blind method in each group of six mice with 10 random 200× fields of view per section. The renal injury was then assessed by calculating the ratio per field of tubular dilatation, tubular cast formation, cellular debris or necrosis of epithelium in the tubular lumen, loss of brush border, loss of nuclei, and basement membrane exfoliation in the renal cortex. For the scores, 0 represents no lesion, 1 indicates minor injury (<25%), 2 indicates mild injury (25–50%), 3 indicates moderate injury (50–75%), and 4 indicates severe injury (>75%).

Apoptosis assay

Paraffin sections were routinely dewaxed, incubated for 20 min with proteinase K at 37 °C and washed with phosphate-buffered saline (PBS). Subsequently, TUNEL assay solution (containing 5 μL of TdT enzyme and 45 μL of fluorescent labeling solution) was added, stained with 4', 6-diamidino-2-phenylindole, washed with PBS, and finally sealed. The sections were then photographed using a confocal microscope (Leica, TCSSP8STED, Weztlar, Germany). Ten random 200× fields were selected for each section,

and TUNEL-positive cells were counted per field. The cells were digested with trypsin and collected by centrifugation, incubated on ice with Annexin V- fluorescein isothiocyanate (labeled by FITC) for 15 min and propidium iodide for 5 min. For cells transfected with smgGDS overexpression lentiviruses, where the vector contained green fluorescent genes with a wavelength similar to that of FITC, the Annexin V-PE/7-ADD apoptosis kit was used. The cells were digested with trypsin, Annexin-PE and 7-AAD were added to the medium and incubated 15 min at room temperature (RT, 25 °C). Then assayed using flow cytometry (CyToFLEX, Beckman Coulter, Brea, California, USA), counting 1×10^5 cells per sample according to the manufacturer's instructions. The gate strategy was shown in Fig. S4.

Renal function measurement

The blood samples were centrifuged at 3000 r/min for 15 min at 4 °C to separate the serum. Next, SCr and BUN levels were measured using the Creatinine (Nanjingjiancheng, Nanjing, China) and Urea Assay Kits (Nanjingjiancheng, Nanjing, China).

Immunofluorescence and immunohistochemistry

For the in vivo sample, the paraffin sections (5 μm) were routinely dewaxed and placed in boiling 1× citrate antigen retrieval solution for 20 min to fully repair the tissue antigen. For the in vitro sample, the cells were seeded on cell slide (Solarbio, Beijing, China) and accepted the corresponding treatment mentioned above. Next, the cells were fixed in 4% paraformaldehyde and permeabilized with 0.3% Triton X-100. Subsequently, the above samples were blocked with 5% normal goat serum in PBS for 1 h at 37 °C. Then, immunostaining was performed by adding mouse anti-smgGDS (1:50, Santa Cruz Biotechnology, Dallas, TX, USA) antibody, rabbit anti-Cadherin16 (1:100, ABclonal, Wuhan, China), and rabbit anti-neutrophil gelatinase-associated lipocalin (NGAL) (1:100, ABclonal, Wuhan, China), incubating overnight at 4 °C, and incubating with fluorescent secondary antibody (1:100–1:200) or peroxidase conjugate secondary antibody for 1 h at 37 °C, visualized by DAB. Lastly, immunofluorescence images were acquired (Leica, TCSSP8STED, Weztlar, Germany), and immunohistochemistry images were captured (Olympus, BX53, Tokyo, Japan). Cells or sections treated with fluorescent or peroxidase-conjugated secondary antibodies only were used as the negative control.

Western blotting

Proteins from the kidney tissues or cells were extracted using RIPA buffer containing a protease and phosphatase inhibitor cocktail. Protein concentrations were measured by the bicinchoninic acid method, then the RIPA buffer was used to align the protein concentrations of each sample. The protein samples added loading buffer with bromophenol blue and heated in a metal bath at 95 °C for 10 min to denature the protein and to expose the protein antigenic sites. Next, the protein samples were separated using 8%–12% SDS-PAGE in running buffer. For the stacking part of the gel, a tension of 70 V was applied until all samples reached the resolving part of the gel, at which point a tension of 100–120 V was applied; finally, electrophoresis was terminated when the protein ladder was completely separated at the level of the target protein weighing. The protein was transferred to a nitrocellulose filter membrane (Pall, Ann Arbor, MI, USA) in Tris-glycine transmembrane buffer on ice bath, and the duration time depended on the molecular weight. Then, the membrane was blocked with blocking buffer for 1 h at RT and incubated with primary antibodies at 4 °C overnight. The next day, the membrane was washed by TBST, then incubated with horseradish peroxidase-conjugated secondary antibody for 1 h at RT and visualized using enhanced chemiluminescence reagent. The antibodies are presented in Table S1.

Quantitative polymerase chain reaction

Total RNA was extracted with TRIzol, and RNA and cDNA synthesis was performed using the PrimeScript RT reagent Kit with gDNA Eraser (TAKARA). Furthermore, real-time quantitative polymerase chain reaction (qPCR) was performed with the ABI 7500 System (Applied Biosciences, LA, CA, USA) using TB Green Premix Ex Taq II (TAKARA). The primers used for qPCR are listed in Table S2.

Eukaryotic transcriptome sequencing and bioinformatics analysis

NC and KD TCKM-1 treated with CDDP (NC + CDDP vs. KD + CDDP) were subjected to transcriptome sequencing (RNA-seq). The transcriptomic and bioinformatic analyses were conducted by Gene-deNovo (Guangzhou, China).

Transmission electron microscopy

WT and *KD* mice were used to establish the CDDP-AKI model, and the kidney cortex was isolated. Next, the tissue was cut into 1 mm^3 sections and promptly fixed in 2.5% glutaraldehyde (4 °C), rinsed in PBS, and re-fixed for 2 h in 1% osmium acid. After dehydrating, soaking, and embedding the sections, the embedded blocks were removed, trimmed to ultra-thin sections (70 nm, Leica UC-7), and sliced in a copper mesh. Next, the sliced sections were electronically stained with lead stain and photographed by using transmission electron microscopy (TEM, Japan Electron Optics Laboratory, JEM1400, Tokyo, Japan) to observe the subcellular features.

Mitochondria membrane potential detection

The mitochondria membrane potential was detected by using 5′,6,6′-tetrachloro-1,1′,3,3′-tetraethylbenzimidazolylcarbocyanine iodide (JC-1) (T3168, Invitrogen). The NC and KD TCMK-1 was seeded into the 35 mm glass bottom dishes. After treatment of the cells, the culture medium was replaced with the working solution of JC-1, and the cells were incubated with JC-1 (10 μg/mL) at 37 °C for 20 min. Gently wash the cells twice with pre-cooled PBS to remove any unbound dye. Then, the images were taken by fluorescence microscope.

Statistics and reproducibility

Statistical analyses were performed using SPSS version 20.0 (IBM SPSS, Chicago, IL, USA) and GraphPad Prism 7 (San Diego, CA, USA), and graphs were constructed using GraphPad Prism 7. Data are expressed as means ± standard deviations. All the Using one-way analysis of variance (ANOVA), we compared the differences between three or more levels of a single variable. Two-way ANOVA with Bonferroni's post hoc correction was performed to compare the effects of the two factors. Lastly, $P < 0.05$ was considered to be indicative of statistical significance.

Data availability

The primers and antibodies information were available in the Supplementary Information. The uncropped images of Western blots are found in Fig. S5. The information of the plasmids, sh-smgGDS(225202) OE-smgGDS(225203), was submitted to Addgene. The raw data and processed data of RNA-seq are available in GEO(GSE275317). The numerical source data are available in Figshare (https://doi.org/10.6084/m9.figshare.26795518). The other datasets generated and/or analyzed during the current study are available from the corresponding author on reasonable request.

Received: 24 January 2024; Accepted: 28 August 2024;
Published online: 05 September 2024

References

1. Levey, A. S. & James, M. T. Acute kidney injury. *Ann. Intern Med*. **167**, ITC66–ITC80 (2017).
2. Bellomo, R., Kellum, J. A. & Ronco, C. Acute kidney injury. *Lancet* **380**, 756–766 (2012).
3. Ronco, C., Bellomo, R. & Kellum, J. A. Acute kidney injury. *Lancet* **394**, 1949–1964 (2019).
4. Wen, L. et al. Selective EZH2 inhibitor zld1039 alleviates inflammation in cisplatin-induced acute kidney injury partially by enhancing RKIP and suppressing NF-κB p65 pathway. *Acta Pharm. Sin.* **43**, 2067–2080 (2022).

5. Pabla, N. & Dong, Z. Cisplatin nephrotoxicity: mechanisms and renoprotective strategies. *Kidney Int* **73**, 994–1007 (2008).
6. Volarevic, V. et al. Molecular mechanisms of cisplatin-induced nephrotoxicity: A balance on the knife edge between renoprotection and tumor toxicity. *J. Biomed. Sci.* **26**, 25 (2019).
7. Jang, H. S. et al. Proximal tubule cyclophilin D regulates fatty acid oxidation in cisplatin-induced acute kidney injury. *Kidney Int* **97**, 327–339 (2020).
8. Guo, J. et al. PERK controls bone homeostasis through the regulation of osteoclast differentiation and function. *Cell Death Dis.* **11**, 847 (2020).
9. Gentilin, E., Simoni, E., Candito, M., Cazzador, D. & Astolfi, L. Cisplatin-induced ototoxicity: Updates on molecular targets. *Trends Mol. Med* **25**, 1123–1132 (2019).
10. Shu, S. et al. Endoplasmic reticulum stress contributes to cisplatin-induced chronic kidney disease via the PERK-PKCδ pathway. *Cell Mol. Life Sci.* **79**, 452 (2022).
11. Frakes, A. E. & Dillin, A. The UPR(ER): Sensor and coordinator of organismal homeostasis. *Mol. Cell* **66**, 761–771 (2017).
12. Balsa, E. et al. ER and nutrient stress promote assembly of respiratory chain supercomplexes through the PERK-eIF2α Axis. *Mol. Cell* **74**, 877–890.e6 (2019).
13. Mao, H., Chen, W., Chen, L. & Li, L. Potential role of mitochondria-associated endoplasmic reticulum membrane proteins in diseases. *Biochem Pharm.* **199**, 115011 (2022).
14. Verfaillie, T. et al. PERK is required at the ER-mitochondrial contact sites to convey apoptosis after ROS-based ER stress. *Cell Death Differ.* **19**, 1880–1891 (2012).
15. Grenier, A. et al. AMPK-PERK axis represses oxidative metabolism and enhances apoptotic priming of mitochondria in acute myeloid leukemia. *Cell Rep.* **38**, 110197 (2022).
16. Li, Y. et al. eIF2α-CHOP-BCl-2/JNK and IRE1α-XBP1/JNK signaling promote apoptosis and inflammation and support the proliferation of Newcastle disease virus. *Cell Death Dis.* **10**, 891 (2019).
17. Kaushik, S. et al. Pitavastatin attenuates cisplatin-induced renal injury by targeting MAPK and apoptotic pathways. *J. Pharm. Pharm.* **71**, 1072–1081 (2019).
18. Krüger, K. et al. Lovastatin prevents cisplatin-induced activation of pro-apoptotic DNA damage response (DDR) of renal tubular epithelial cells. *Toxicol. Appl Pharm.* **292**, 103–114 (2016).
19. Kudo, S. et al. SmgGDS as a crucial mediator of the inhibitory effects of statins on cardiac hypertrophy and fibrosis: Novel mechanism of the pleiotropic effects of statins. *Hypertension* **67**, 878–889 (2016).
20. Minami, T. et al. Statins up-regulate SmgGDS through β1-integrin/Akt1 pathway in endothelial cells. *Cardiovasc Res.* **109**, 151–161 (2016).
21. Oesterle, A., Laufs, U. & Liao, J. K. Pleiotropic effects of statins on the cardiovascular system. *Circ. Res.* **120**, 229–243 (2017).
22. Tanaka, S. et al. Statins exert the pleiotropic effects through small GTP-binding protein dissociation stimulator upregulation with a resultant Rac1 degradation. *Arterioscler Thromb. Vasc. Biol.* **33**, 1591–1600 (2013).
23. Yamamoto, T. et al. Purification and characterization from bovine brain cytosol of proteins that regulate the GDP/GTP exchange reaction of smg p21s, ras p21-like GTP-binding proteins. *J. Biol. Chem.* **265**, 16626–16634 (1990).
24. Nogi, M. et al. Small GTP-binding protein GDP dissociation stimulator prevents thoracic aortic aneurysm formation and rupture by phenotypic preservation of aortic smooth muscle cells. *Circulation* **138**, 2413–2433 (2018).
25. Wang, T. et al. Estradiol-mediated small GTP-binding protein GDP dissociation stimulator induction contributes to sex differences in resilience to ferroptosis in takotsubo syndrome. *Redox Biol.* **68**, 102961 (2023).
26. Asiri, A. et al. Mutated RAP1GDS1 causes a new syndrome of dysmorphic feature, intellectual disability & speech delay. *Ann. Clin. Transl. Neurol.* **7**, 956–964 (2020).
27. Sánchez-Vera, I. et al. The prohibitin-binding compound fluorizoline activates the integrated stress response through the eIF2α Kinase HRI. *Int J. Mol. Sci.* **24**, 8064 (2023).
28. Muñoz, J. P. et al. Mfn2 modulates the UPR and mitochondrial function via repression of PERK. *EMBO J.* **32**, 2348–2361 (2013).
29. Zhang, K. et al. The PERK-EIF2α-ATF4 signaling branch regulates osteoblast differentiation and proliferation by PTH. *Am. J. Physiol. Endocrinol. Metab.* **316**, E590–E604 (2019).
30. Naveau, M. et al. Roles of yeast eIF2α and eIF2β subunits in the binding of the initiator methionyl-tRNA. *Nucleic Acids Res.* **41**, 1047–1057 (2013).
31. Orwick, A. et al. Lung cancer-kidney crosstalk induces kidney injury, interstitial fibrosis, and enhanced cisplatin-induced nephrotoxicity. *Am. J. Physiol Renal Physiol* (2023).
32. Hao, L. et al. ATF4 activation promotes hepatic mitochondrial dysfunction by repressing NRF1-TFAM signalling in alcoholic steatohepatitis. *Gut* **70**, 1933–1945 (2021).
33. Kumar, V. & Maity, S. ER stress-sensor proteins and ER-mitochondrial crosstalk-signaling beyond (ER) stress response. *Biomolecules* **11**, 173 (2021).
34. Tapella, L. et al. Protein synthesis inhibition and loss of homeostatic functions in astrocytes from an Alzheimer's disease mouse model: a role for ER-mitochondria interaction. *Cell Death Dis.* **13**, 878 (2022).
35. Zhong, Y. et al. Inhibition of ER stress attenuates kidney injury and apoptosis induced by 3-MCPD via regulating mitochondrial fission/fusion and Ca(2+) homeostasis. *Cell Biol. Toxicol.* **37**, 795–809 (2021).
36. Zhou, H. Y., Sun, Y. Y., Chang, P. & Huang, H. C. Curcumin Inhibits Cell Damage and Apoptosis Caused by Thapsigargin-Induced Endoplasmic Reticulum Stress Involving the Recovery of Mitochondrial Function Mediated by Mitofusin-2. *Neurotox. Res.* **40**, 449–460 (2022).
37. Chino, H. & Mizushima, N. ER-Phagy: Quality control and turnover of endoplasmic reticulum. *Trends Cell Biol.* **30**, 384–398 (2020).
38. Ferro-Novick, S., Reggiori, F. & Brodsky, J. L. ER-Phagy, ER Homeostasis, and ER quality control: Implications for disease. *Trends Biochem Sci.* **46**, 630–639 (2021).
39. García-Torres, D. & Fierke, C. A. The chaperone SmgGDS-607 has a dual role, both activating and inhibiting farnesylation of small GTPases. *J. Biol. Chem.* **294**, 11793–11804 (2019).
40. Shimizu, H., Toma-Fukai, S., Kontani, K., Katada, T. & Shimizu, T. GEF mechanism revealed by the structure of SmgGDS-558 and farnesylated RhoA complex and its implication for a chaperone mechanism. *Proc. Natl Acad. Sci. USA* **115**, 9563–9568 (2018).
41. Lanning, C. C., Ruiz-Velasco, R. & Williams, C. L. Novel mechanism of the co-regulation of nuclear transport of SmgGDS and Rac1. *J. Biol. Chem.* **278**, 12495–12506 (2003).
42. Brandt, A. C., Koehn, O. J. & Williams, C. L. SmgGDS: An emerging master regulator of prenylation and trafficking by small GTPases in the Ras and Rho Families. *Front Mol. Biosci.* **8**, 685135 (2021).
43. Hwang, J. & Qi, L. Quality control in the endoplasmic reticulum: Crosstalk between ERAD and UPR pathways. *Trends Biochem Sci.* **43**, 593–605 (2018).
44. Zhou, Y. et al. Porcine epidemic diarrhea virus activates PERK-ROS axis to benefit its replication in Vero E6 cells. *Vet. Res.* **54**, 9 (2023).
45. Novoa, I., Zeng, H., Harding, H. P. & Ron, D. Feedback inhibition of the unfolded protein response by GADD34-mediated dephosphorylation of eIF2alpha. *J. Cell Biol.* **153**, 1011–1022 (2001).
46. Liu, X. et al. DRD4 (dopamine D4 Receptor) mitigate abdominal aortic aneurysm via decreasing P38 MAPK (mitogen-activated protein kinase)/NOX4 (NADPH oxidase 4) axis-associated oxidative stress. *Hypertension* **78**, 294–307 (2021).

47. Xu, S. et al. Nuclear farnesoid X receptor attenuates acute kidney injury through fatty acid oxidation. *Kidney Int* **101**, 987–1002 (2022).
48. Chu, H. et al. Targeting highly pathogenic coronavirus-induced apoptosis reduces viral pathogenesis and disease severity. *Sci. Adv.* **7**, eabf8577 (2021).
49. Sharma, V. et al. eIF2α controls memory consolidation via excitatory and somatostatin neurons. *Nature* **586**, 412–416 (2020).
50. Sidrauski, C., McGeachy, A. M., Ingolia, N. T. & Walter, P. The small molecule ISRIB reverses the effects of eIF2α phosphorylation on translation and stress granule assembly. *Elife* **4**, e05033 (2015).
51. Chen, J. et al. EGF receptor-dependent YAP activation is important for renal recovery from AKI. *J. Am. Soc. Nephrol.* **29**, 2372–2385 (2018).

Acknowledgements

This study was supported by National Natural Science Foundation of China General Program (No.82170508), National Natural Science Foundation of China Youth Program (No.82300546), 535 Talent Project of First Affiliated Hospital of Kunming Medical University (No. 2023535Q06), and Yangzhou University International Academic Exchange Fund.

Author contributions

Y.Y.: Conceptualization, methodology, project administration, formal analysis, data curation, writing—original draft, and writing—review and editing. T.X.: Conceptualization, methodology, administration, formal analysis, writing—review and editing. T.W.: Conceptualization, methodology, administration, formal analysis, writing—review and editing. X.C.: Investigation, methodology, and data curation. Z.M.: data curation. B.Z.: data curation. D.N.: data curation. R.S.: Methodology and software. X.L.: Conceptualization, methodology, data curation, and writing—review and editing. D.W.: Conceptualization, funding acquisition, data curation, supervision, and writing—review and editing.

Competing interests

The authors declare no competing interests. The corresponding author, Daxin Wang, had full access to all data in the study and had the final responsibility for the decision to submit for publication.

Ethics approval

All institutional and national guidelines for the care and use of laboratory animals were followed. All animal experiments were approved by the Ethics Committee of Yangzhou University (approval no. 202210006) and were conducted in accordance with the National Institutes of Health Guidelines for the Care and Use of Laboratory Animals.

Additional information

Supplementary information The online version contains supplementary material available at https://doi.org/10.1038/s42003-024-06792-4.

Correspondence and requests for materials should be addressed to Xuesong Liu or Daxin Wang.

Peer review information *Communications biology* thanks Jun Liu and the other, anonymous, reviewer(s) for their contribution to the peer review of this work. Primary Handling Editor: Christina Karlsson Rosenthal. A peer review file is available.